Pickup coupling contribution to the optical model potential for 30.3 MeV protons and neutrons on ^{40}Ca

N. Keeley[*]

National Centre for Nuclear Research, ul. Andrzeja Sołtana 7, 05-400 Otwock, Poland

R. S. Mackintosh[†]

School of Physical Sciences, The Open University, Milton Keynes MK7 6AA, UK

We study the dynamic polarization potentials (DPPs) for 30.3 MeV protons and neutrons scattering from ^{40}Ca that are generated by the coupling to deuteron channels. In this way we resolve unexpected differences from the general properties of such DPPs found in similar cases for lighter targets. It turns out that the contribution of particular states to the real part can change considerably with Q value, coming close to changing sign. One consequence is the surprising result presented in Mackintosh and Keeley [Phys. Rev. C **97**, 069901(E) (2018)], which is investigated here. The Q-value dependence of the DPPs also contributes to a substantial difference between the optical model potential for protons and neutrons, there being substantially different Q values for ^{40}Ca (n, d) and ^{40}Ca (p, d) pickup reactions. The DPP calculations also enable a study of the dynamical nonlocality (distinct from exchange nonlocality) arising from pickup coupling. The characteristic properties of the DPPs for both protons and neutrons arising from nucleon pickup are also presented for incident nucleons at 25, 35, 40, and 45 MeV. All these properties vary with energy in a consistent way, including a change in the rms radius of the real potential, which, together with the general undularity of the DPP, shows that the pickup contributions cannot be represented by renormalizing a folding model potential.

I. INTRODUCTION

It is known that the elastic scattering of protons on nuclei is strongly influenced by pickup coupling to deuteron channels, see Ref. [1] and references therein. The resulting effective contribution to the optical model potential (OMP) is such that the OMP can no longer be accurately represented as a smooth ("Woods-Saxon-like") l-independent radial function. Whether l dependence or unsmoothness is the more appropriate representation is debatable; for any l-dependent potential there is always a (nonsmooth) l-independent potential with the same S-matrix S_{lj} and therefore the same observables. What has been established is that the effects of pickup coupling can be represented by a local and l-independent potential that is not smooth and cannot be represented as a uniform renormalization of a folding model potential based on a local density model. For many light nuclei, the pickup channel coupling effects are found to make an overall repulsive contribution to the real central potential as well as a strongly absorptive contribution to the imaginary central term. There are also substantial contributions to the real and imaginary spin-orbit interactions. Fairly recent calculations exhibiting these features are Ref. [2] for ^{10}Be, Ref. [3] for ^{8}He, and Ref. [4] for ^{6}He. These are all light nuclei with one or a few hole states in the residual nucleus. In each case the Q values are relatively small in magnitude and this may have some bearing on why the effects we shall describe below have not been noted before.

Unlike the cases of Refs. [2–4], Ref. [1] found that coupling to deuteron pickup channels led to attraction for both protons and neutrons scattering from ^{16}O. In this case there was also a large difference between the pickup contributions for protons and neutrons at the same energy. The magnitude of the attraction for protons was substantial, markedly changing the overall radial form of the real potential. This attractive effect was in contrast to what had been found [5] for the case of protons on ^{40}Ca where coupling to the $\frac{3}{2}^{+}$ ground state, GS, of ^{39}Ca (pickup of a $\frac{3}{2}^{+}$ neutron) generated repulsion and the inclusion of $\frac{5}{2}^{+}$ states increased that repulsion. The radial form of the dynamical polarization potential (DPP) when the $\frac{5}{2}^{+}$ states were included was similar to that for the case with coupling to the $\frac{3}{2}^{+}$ ground state only. These new results suggested that the DPPs for ^{40}Ca were similar to those for the light nuclei mentioned above rather than ^{16}O. However, it was discovered that some of the $\frac{5}{2}^{+}$ results for ^{40}Ca were spurious due to an error in the version of the CRC code that was used. It was subsequently found [6] that including the complete set of pickup states generated a much smaller degree of repulsion than the $\frac{3}{2}^{+}$ state alone, as quantified by ΔJ_R. In fact the DPP had a substantial attractive region near the nuclear center, although there was repulsion at somewhat

[*]nicholas.keeley@ncbj.gov.pl
[†]raymond.mackintosh@open.ac.uk

TABLE I. For protons scattering from ^{40}Ca at 30.3 MeV/nucleon, volume integrals ΔJ (in MeV fm^3) of the four components of the DPP induced by (p, d) coupling. The ΔR_{rms} column gives the change in rms radius of the real central component (in fm). The final three columns present, respectively, the change in the total reaction cross section induced by the coupling, the integrated cross section to the specific coupled reaction channels, and the ratio R defined in the text. Note that negative ΔJ_R corresponds to repulsion. The excitation energies of the states, in MeV, are given in the text. The quantities Δ(Reac CS) and State CS are given in mb.

Label	States coupled	ΔJ_R	ΔJ_{IM}	ΔJ_{RSO}	ΔJ_{IMSO}	ΔR_{rms}	Δ(Reac CS)	State CS	R
state 1	1	−12.88	14.57	0.848	−0.291	0.0331	51.63	7.93	3.55
twostate	1, 2	−19.04	23.13	1.416	−0.477	0.0392	80.33	13.92	3.47
gsh7	1, 2, 3	−17.63	25.07	1.392	−0.478	0.0450	86.43	14.73	3.45
fourstate	1, 2, 3, 4	−18.23	46.40	2.447	−0.658	0.0645	129.53	16.96	2.79
fivestate	1, 2, 3, 4, 5	−13.44	54.67	3.330	−0.722	0.0528	141.13	16.23	2.58
gsplus5h	1, 4	−16.72	30.27	1.720	−0.323	0.0597	95.63	12.04	3.16
state 6	6	−0.72	2.890	0.147	0.068	0.0045	12.54	1.15	4.34
All1	1, 2, 3, 4*(6.5132 MeV)	−7.37	59.99	3.756	−1.736	0.0338	147.13	15.22	2.45

greater radii. The overall radial form of the full DPP was no longer similar to that due to coupling to just the $\frac{3}{2}^+$ state. This raised the whole question of the way the DPP depends on such factors as the l transfer, Q value, etc., and the present work is, in part, an attempt to gain some understanding of these matters. There is a strong motivation: the effect of the pickup coupling is substantial, and represents a contribution to the nucleon-nucleus interaction which is arguably beyond the reach of folding models based on an underlying local density approximation, particularly for lighter nuclei for which the surface region has a dominant influence on scattering. In addition, Ref. [1] found a large difference between the DPPs due to pickup for protons and neutrons. This implies a large difference between proton and neutron OMPs for the $T = 0$ nucleus ^{16}O. If this is more generally true, then it is significant, since the difference between the proton and neutron OMPs is essential for determining $\mathbf{t} \cdot \mathbf{T}$ terms for $T \neq 0$ nuclei.

In the cases referenced above and in this work, the pickup contributions are determined as follows: the elastic channel S-matrix S_{lj} from a coupled reaction channel (CRC) calculation is subject to $S_{lj} \rightarrow V(r) + \mathbf{l} \cdot \mathbf{s} V_{\mathrm{SO}}(r)$ inversion and the difference between the resulting potential and the "bare potential," the elastic channel potential of the CRC calculation, is identified as a local representation of the DPP due to the coupling; see Ref. [3] for more details. The formal DPP is both l dependent and nonlocal, see Refs. [7–10]. This channel-coupling nonlocality is distinct from the nonlocality due to exchange [11] which is commonly represented phenomenologically [12,13]. We refer to the nonlocality arising from channel coupling as dynamical nonlocality, see also Ref. [10]. Some of the undulatory ("wavy") properties of local and l-independent DPPs can be attributed to the underlying l-dependence of the formal DPP [7–9]. In what follows all CRC calculations were performed with the code FRESCO [14].

II. DPP CALCULATIONS FOR 30.3 MEV PROTON ELASTIC SCATTERING

Coupling to the full set of states of ^{39}Ca listed in Ref. [5], referred to in what follows as PRC85, gives rise to DPPs that have radial forms very different to the form generated

by coupling to just the $\frac{3}{2}^+$ ground state (GS) [6]. This has implications for all determinations of reaction channel contributions to OMPs and in order to achieve some understanding of this, DPPs have been determined for various combinations of coupled states ranging from the GS only to the complete set of PRC85. The characteristics of the DPPs generated by coupling to particular sets of states of ^{39}Ca are presented in Table I. In this table the changes in the potential are quantified in terms of the changes in the volume integrals, as defined and normalized in Ref. [9]. Thus ΔJ_R, ΔJ_{IM}, ΔJ_{RSO}, and ΔJ_{IMSO} are, respectively, the changes in the real central, imaginary central, real spin-orbit, and imaginary spin-orbit components while ΔR_{rms} is the change induced by the coupling in the rms radius of the real central component. The radial forms of the DPPs will be presented in Sec. IV.

To facilitate the discussion, we refer to the main set of states of ^{39}Ca considered in PRC85 by number, ordered by excitation energy:

(1) $\frac{3}{2}^+$ (0.0); (2) $\frac{1}{2}^+$ (2.467); (3) $\frac{7}{2}^-$ (2.796);
(4) $\frac{5}{2}^+$ (5.6175); (5) $\frac{5}{2}^+$ (7.3148); (6) $\frac{5}{2}^+$ (8.5148)

States 4, 5, and 6 are each, in fact, collected groups of three states, suitably weighted, see PRC85. Collecting states of the same spin-parity but different excitation energies into groups with appropriate weighting is a computationally economical means of calculating DPPs. Such weighting leads to DPPs that are identical to those derived from calculations including the full set of states, see Ref. [6], where it was demonstrated that the DPP resulting from a CRC calculation coupling all nine $\frac{5}{2}^+$ states considered in PRC85 (plus states 1–3) was graphically almost indistinguishable from that derived from a calculation coupling the three lumped $\frac{5}{2}^+$ states (4–6) together with states 1–3.

In this work we refer to the calculation which couples states 1–6 as "Fig3dash" (since the corresponding DPP is denoted by the dashed curve in Fig. 3 of Ref. [5]). We further refer to a calculation where the nine $\frac{5}{2}^+$ states were lumped into a single state at the suitably weighted excitation energy of 6.5132 MeV as "All1" (states 1–3 were of course also included). The DPP derived from All1 is graphically almost indistinguishable

TABLE II. For protons scattering from ^{40}Ca at 30.3 MeV/nucleon, volume integrals ΔJ (in MeV fm^3) of the two central terms of the DPP induced by (p, d) coupling. Negative ΔJ_R corresponds to repulsion. In each pair of DPPs, the upper line presents the sums of the DPPs for the indicated states, or sets of states, with no mutual coupling. The lower line of each pair gives the DPPs calculated with all states included in the same CRC calculation without mutual coupling. The last column refers to the figure where the respective DPPs are presented, see Sec. IV.

States coupled	ΔJ_R	ΔJ_{IM}	State CS	Figure
state 1, state 2 summed	-16.53	20.26	14.44	Fig. 2
Twostate	-19.04	23.13	13.92	
state 1, state 4 summed	-15.89	24.99	12.84	Fig. 3
gsplus5h	-16.72	30.27	12.04	
gsh7, state 4 summed	-20.99	35.42	19.64	Fig. 4
Fourstate	-18.23	46.40	16.96	
Fourstate, state 5 summed	-18.98	49.98	18.56	Fig. 5
Fivestate	-13.44	54.67	16.23	
Fivestate, state 6 summed	-14.16	57.55	17.38	Fig. 6
Fig3dash	-7.77	59.74	15.13	

from that of both Fig3dash and the calculation coupling all nine $\frac{5}{2}^+$ states. The numerical results are also almost identical for all three calculations so we only give those appertaining to All1 in Table I. In what follows we shall sometimes refer to the DPP for Fig3dash and sometimes to that for All1, depending on which is most appropriate to the context of the discussion. However, it should be borne in mind that they are for all practical purposes identical. In Tables I and III, "4*(x MeV)" indicates a single lumped $\frac{5}{2}^+$ state at x MeV including the strength of all the $\frac{5}{2}^+$ states.

In Table I the quantity R is the ratio of the change in reaction cross section due to the coupling, Δ(Reac CS), to the change due to coupling in the volume integral of the imaginary central potential, ΔJ_{IM}:

$$R = \frac{\Delta(\text{ReacCS})}{\Delta J_{IM}}. \quad (1)$$

R varies over a much smaller range than Δ(Reac CS) or ΔJ_{IM} separately. "State CS" is the (p, d) cross section to the pickup states specified in column 2. It gives a measure of the coupling and varies much less than the corresponding ΔJ_{IM}.

In every case where an additional state is added, the magnitude of ΔJ_{IM} increases. This property of the inverted potentials is in accord both with intuition and the formal nonlocal DPP, see p. 58 of Satchler [9]. The imaginary spin-orbit volume integral, ΔJ_{IMSO}, also increases as states are added (with the possible exception of state 6), as does Δ(Reac CS). There is no such systematic increase in ΔJ_R as additional states are coupled, as is evident from Table I, and this is important for the present study. In part, this reflects the fact that the real component of the DPP has both positive and negative radial regions. The DPP is predominantly repulsive for coupling to the first two states but in Sec. IV we show that higher lying states generate successively more attraction as they are included.

III. ADDITIVITY AND DYNAMICAL NONLOCALITY

The formal DPPs arising from the coupling to specific states are both l dependent and dynamically nonlocal.

Dynamical nonlocality is distinct from nonlocality arising from exchange [10]. In the present calculations there is no coupling between the states of ^{39}Ca that are coupled to the elastic channel, and this makes it possible to get a measure of the dynamical nonlocality. We say that a local potential is "S-matrix equivalent" to a nonlocal potential if it leads to the same S_{lj} (and hence the same observables.) If state 1 and state 2 are each coupled to the ground state, but not coupled to each other, then the formal [7–9] nonlocal DPP, $\mathcal{V}_{12}$, will be the sum, $\mathcal{V}_1 + \mathcal{V}_2$, of the nonlocal DPPs $\mathcal{V}_1$ and $\mathcal{V}_2$ generated by coupling to state 1 and state 2 alone, respectively. However, the local S-matrix equivalent of $\mathcal{V}_{12}$ is not the sum of the local equivalents of $\mathcal{V}_1$ and $\mathcal{V}_2$. We refer to this as the "nonadditivity of local equivalents" and it provides a measure of dynamically induced nonlocality. This property was exploited in Ref. [3] and discussed in more detail in Ref. [15].

The nonadditivity can be evaluated by a point-by-point comparison of the local DPP for a particular set of states with the sum of the individual local DPPs for each state. Alternatively, the volume integrals may be compared. Both comparisons are possible for various combinations of states. For example, the sums of the volume integrals for the cases "fivestate" and "state 6" may be compared with the same volume integrals for "Fig3dash."

As a particular example, if there is no dynamical nonlocality, then the ΔJ values should be the same for the cases S and T defined as follows: case S: The sum of the "fivestate" DPP and the "state 6" DPP; case T: The "Fig3dash" DPP; in this case, "fivestate" and "state 6" are included together in the CRC calculation but not mutually coupled.

In the order of Table I: The ΔJ values in MeV fm^3 for case S are -14.16, 57.56, 3.477, -0.654. The corresponding values for case T are -7.77, 59.74, 3.708, -1.719.

The difference in ΔJ_R between -14.16 MeV fm^3 and -7.77 MeV fm^3 occurs just for the case in which the "Fig3dash" real central DPP exhibits a substantial change in radial shape. State 6 makes a disproportionate contribution to the DPP, and the nonadditivity is particularly evident in the real central term.

Table II compares the volume integrals for the central potentials for five cases, including the cases S and T just

mentioned. There is no coupling between pickup states in any of the calculations. In each of the five comparisons, the first line gives the sum of the volume integrals for the DPPs due to the two specified states or sets of states, labeled as in Table I; the second line is for the DPP arising when all the same pickup states are coupled in a single calculation. In all cases there is a substantial difference between the "summed" value and the "together" value beneath it. In the first two cases the repulsion due to the coupling is increased when "together" and decreased in the other cases. In all cases absorption due to coupling is increased when the states are included together: ΔJ_{IM} is greater when the coupled channels are included in the same calculation, but the cross section to the pickup states is less. For example, for the top case, while $23.13 > 20.26$, $13.92 < 14.44$, this is not the relationship that might be expected. The radial dependence of the additivity of the DPPs is presented in the next section.

IV. RADIAL PROPERTIES OF DPPS FOR PROTONS

In this section we present the radial dependence of the DPPs for proton scattering induced by various combinations of couplings. At this point it is also convenient to address the question that naturally arises concerning the choice of bare potential. The studies of Sec. III concerning nonlocality require a fixed bare potential. Moreover, it is frequently impractical to search on the parameters of the bare potential to fit the elastic-scattering observables when all couplings are included. Fortunately, it turns out [16] that the DPPs induced by (p, d) couplings are, to a surprising degree, independent of the bare potentials. To enable comparison with the earlier work, we retain the bare potential used in PRC85. In Fig. 1 we compare this bare potential with the inverted potentials for coupling to the $\frac{3}{2}^+$ ground state of ^{39}Ca and to the All1 set of states. For each case, the components of the DPP are the differences between the corresponding terms for the inverted and bare potentials. For all other cases only the DPPs will be presented graphically.

A. Dynamical nonlocality: The additivity of DPPs

We first present figures that compare the "summed" and "together" DPPs for the following cases in the order of Table II:

(1) states 1 and 2; Fig. 2
(2) states 1 and 4; Fig. 3
(3) states 1–3 (gsh7) and state 4; Fig. 4
(4) states 1–4 (fourstate) and state 5; Fig. 5
(5) states 1–5 (fivestate) and state 6; Fig. 6

In each of the five figures the difference between the central parts of the "summed" and "together" DPPs is very small beyond 3 fm. For this reason, the changes in volume integrals in Table II do not reflect the considerable changes for $r \leqslant 3$ fm. The relatively small difference for $r > 3$ fm is expected since the effect of the dynamical nonlocality will operate in the radial range where the DPP is large, i.e., $r \leqslant 3$ fm. Figure 6 shows that the very small DPP for state 6 added to the fivestate DPP makes very little difference, but when this
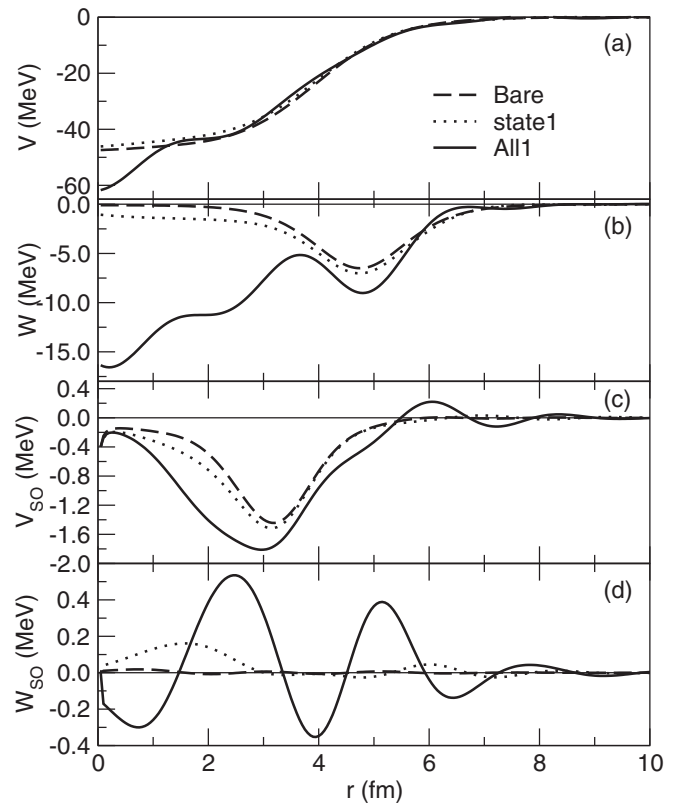

FIG. 1. For 30.3 MeV protons on ^{40}Ca, the dashed lines present the bare potential and the dotted lines present the inverted potential for coupling to the $\frac{3}{2}^+$ ground state. The solid lines represent the inverted potential for coupling to the complete set of states in the All1 grouping. The panels present, from the top down, the real central, imaginary central, real spin-orbit, and imaginary spin-orbit components.

state is included in the coupling scheme to give the complete (Fig3dash) calculation, the difference is conspicuous.

B. Concerning the radial form of DPPs

The DPPs in Figs. 2 to 6 do not represent a simple renormalization of the bare potential and are somewhat undulatory, indicating an underlying l dependence. The validity of the DPPs calculated here is supported by the results in Ref. [16]. Figure 7 compares the DPPs for coupling to the two $\frac{5}{2}^+$ states, states 5 and 6, and the general shapes are very similar. The magnitudes of the central terms of the DPP for state 5 are systematically somewhat larger than those for state 6, consistent with the ratio of spectroscopic factors: That for state 5 is greater than that for state 6 by a factor of 1.17. Further differences may be due to the 1.2 MeV difference in Q value.

C. Test calculations progressing to All1 properties

The radial form of the real DPP for the All1 case differs markedly from that resulting from coupling to the three lowest states in ^{39}Ca, gsh7 in the nomenclature of Table I, for which it was repulsive at almost all radii. Adding coupling to the
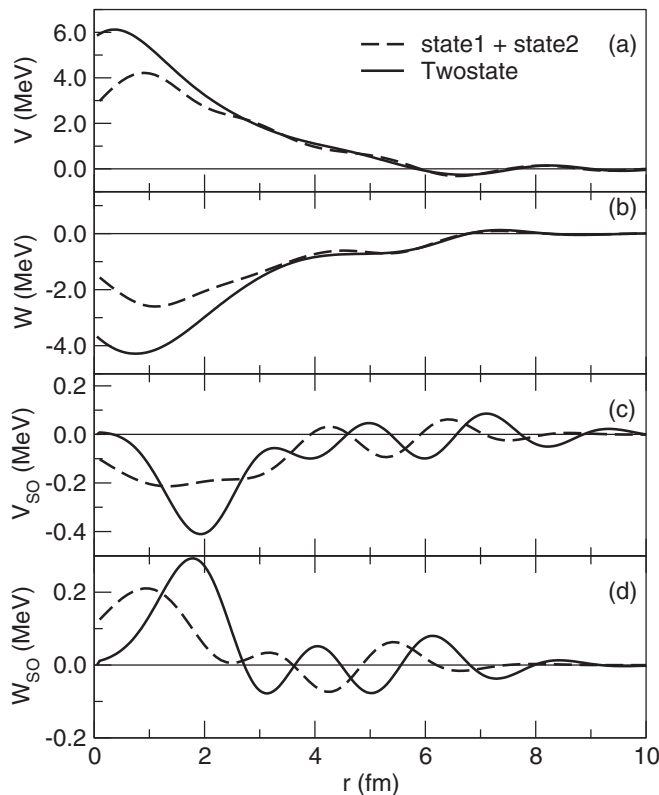
FIG. 2. For 30.3 MeV protons on ^{40}Ca, the solid lines present the DPP due to coupling to the ground state and to the $\frac{1}{2}^+$ state at 2.467 MeV. The dashed lines present the sum of the DPPs for each of the same states separately. The panels present, from the top down, the real central, imaginary central, real spin-orbit, and imaginary spin-orbit components. Note the roughly 10 times expansion of the scale for the spin-orbit components.

FIG. 3. For 30.3 MeV protons on ^{40}Ca, the solid lines present the DPP due to coupling to the ground state and state 4, 5.6175 MeV $\frac{5}{2}^+$. The dashed lines present the sum of the DPPs due to each of the same states coupled separately. The panels present, from the top down, the real central, imaginary central, real spin-orbit, and imaginary spin-orbit components. Note the roughly 10 times expansion of the scale for the spin-orbit components.

lowest lumped $\frac{5}{2}^+$ state at 5.6175 MeV ("fourstate") did not alter the situation much, leading to the solid line in Fig. 4. Addition of the second lumped $\frac{5}{2}^+$ state at 7.3148 MeV ("fivestate") had a significant effect but still did not lead to attraction in the nuclear interior; Fig. 6 shows dramatically the gap that needs to be filled (as stated earlier, the "Fig3dash" and "All1" DPPs are graphically almost indistinguishable). Figure 6 clearly shows that it is the addition of the final lumped $\frac{5}{2}^+$ state, that at 8.5148 MeV, which is responsible for the dramatic change in sign of the real part of the DPP at small radii.

In order to gain some understanding of this effect whereby coupling to the high-lying $\frac{5}{2}^+$ states greatly reduces the repulsion, generating a region of attraction near the nuclear center, a series of test calculations was carried out in which the same states were coupled as for the All1 calculation but the excitation energy of the single $\frac{5}{2}^+$ state was varied. In the first of these calculations the excitation energy was 3 MeV compared with 6.5132 MeV for the All1 case. We refer to this case as "test1" and the numerical characteristics of the DPP are given in Table III. The radial shapes of the test1 and All1 DPPs are compared in Fig. 8. The change in excitation energy of the pickup states does not change the basic form of
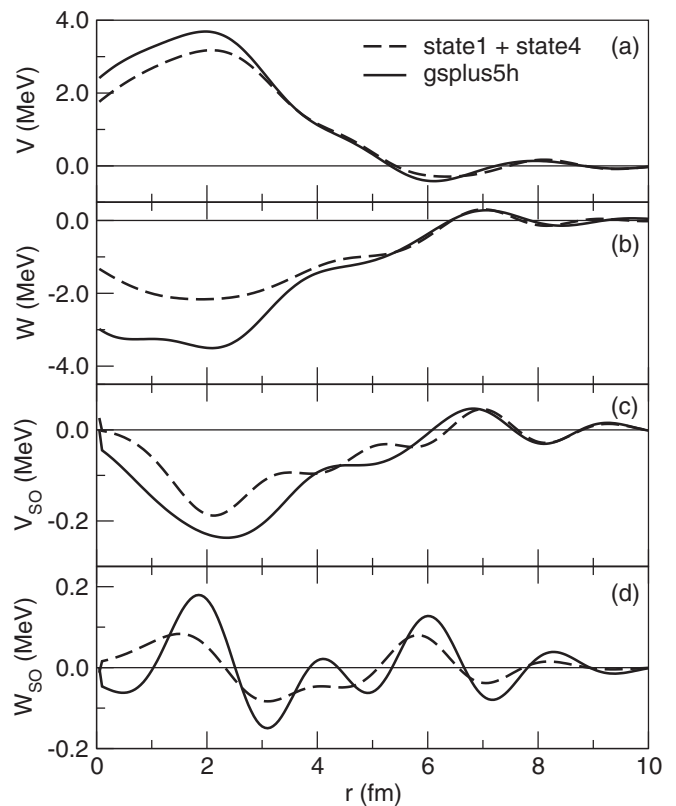
the imaginary central DPP, but the real central DPP is subject to major qualitative change. In particular, there is a complete shape change for $r < 1$ fm, although this region has a limited effect on ΔJ_R. The test1 behavior suggests that the sensitivity of the DPP to the details of the coupling is part of a pattern.

A further sequence of test calculations were therefore performed. Test2 raised the excitation energy of the lumped $\frac{5}{2}^+$ state to 4 MeV, test3 to 5 MeV, test4 to 6 MeV, and testX to 10 MeV. The resulting DPPs are presented in Figs. 8 and 9; the corresponding numerical quantities are given in Table III. It will be seen that the test4 case leads to values of ΔJ_R, etc., close to those for All1, with the values for the other tests varying in a remarkably regular way as the energy of the lumped state is increased. TestX shows that the trend continues to unreasonable values of the excitation energy, showing that the net repulsion of the other cases almost becomes net attraction when the excitation energy of the lumped $\frac{5}{2}^+$ state reaches 10 MeV. Figure 9 compares the testX potential with the All1 potential, and it will be seen that the absorptive potential falls as the coupled $\frac{5}{2}^+$ state rises to 10 MeV, presumably due to momentum mismatch.

One consequence of the behavior found here is that reliable evaluations of DPPs and coupling effects require care in the
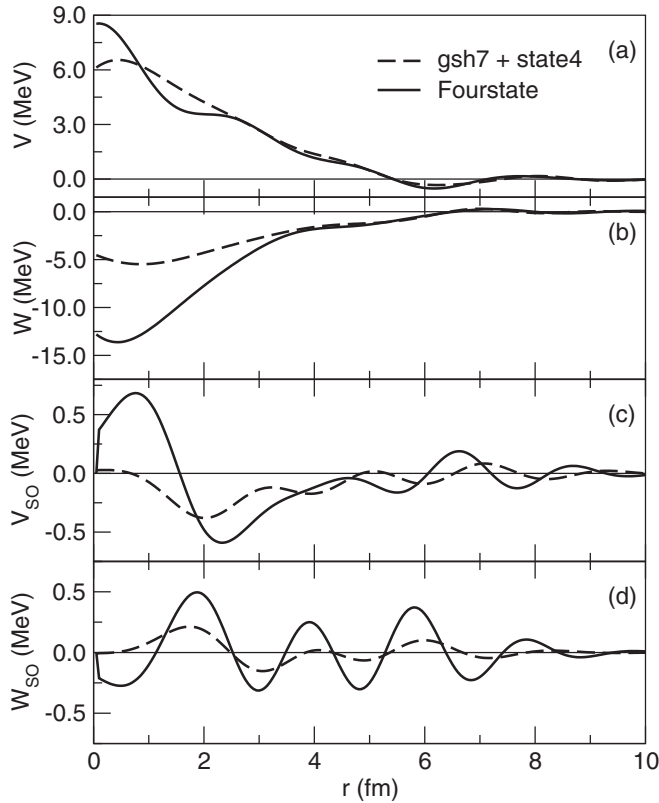
FIG. 4. For 30.3 MeV protons on ^{40}Ca, the solid lines present the DPP due to coupling to the four lowest energy states ("fourstate"); the dashed lines present the sum of the DPPs due to coupling to the first three states ("gsh7") and the DPP due to coupling to state four, $\frac{5}{2}^+$ at 5.6175 MeV. The panels present, from the top down, the real central, imaginary central, real spin-orbit, and imaginary spin-orbit components.

FIG. 5. For 30.3 MeV protons on ^{40}Ca, the solid lines present the DPP due to coupling to the five lowest energy states ("fivestate"); the dashed lines present the sum of the DPPs due to coupling to the first four states ("fourstate") and the DPP due to coupling to state five, $\frac{5}{2}^+$ at 7.3148 MeV. The panels present, from the top down, the real central, imaginary central, real spin-orbit, and imaginary spin-orbit components.

choice of channels coupled and tests of the sensitivity of results to the nature of the coupling employed.

D. General properties of the DPP for 30.3 MeV proton elastic scattering on ^{40}Ca

(1) Coupling to just the three lowest states of ^{39}Ca would lead to the erroneous conclusion that the pickup coupling effect on the real potential was substantial and almost uniformly repulsive. A more complete calculation leads to the conclusion that the overall repulsion is much smaller, and becomes attraction at the nuclear center.

(2) Pickup channel coupling induces a substantial increase in the rms radius of the real central potential, affecting any extraction of nuclear radii from elastic scattering.

(3) The imaginary central DPP has a form unlike the usual phenomenological forms, and in particular has an emissive region around 6.5 fm, although in this case the full potential does not.

(4) Coupling to pickup channels contributes to both the real and imaginary spin-orbit potentials. The imaginary spin-orbit DPP (and potential) does have an
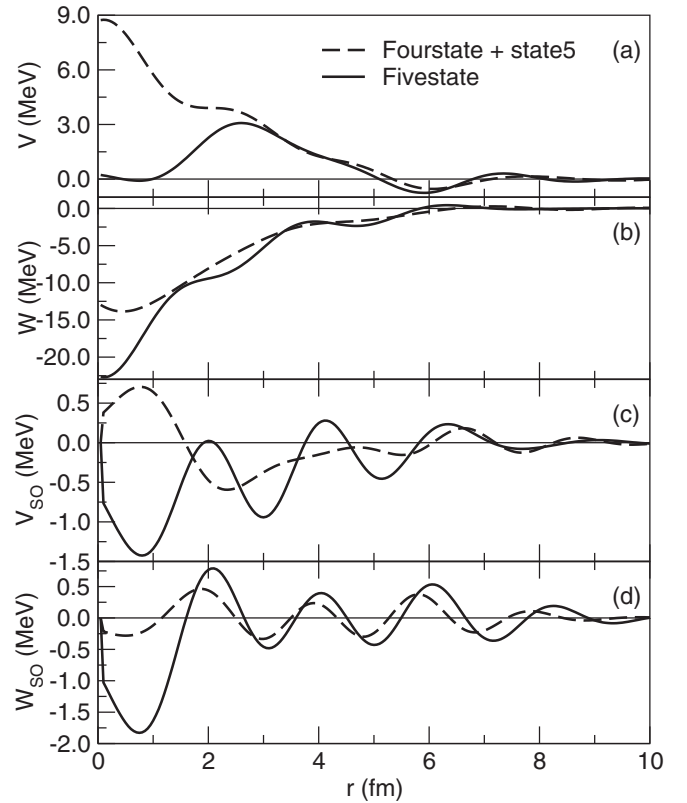
emissive region. The significance of this is discussed in Sec. VIII.

(5) The real spin-orbit DPP has a volume integral that is almost constant across the series of tests, test1 to testX, whereas the imaginary spin-orbit increases in magnitude in a regular way as the energy of the lumped pickup state increases.

(6) The real central DPP has features that could not be represented by renormalizing a folding model potential based on a local density model. In particular, renormalisation would miss the effect pickup coupling has on the rms radius.

V. PICKUP EFFECTS FOR NEUTRON ELASTIC SCATTERING

Reference [1] showed that coupling to nucleon pickup channels made significantly different contributions to the neutron and proton OMPs for scattering from the $T = 0$ nucleus ^{16}O. The effect is likely to be greater for ^{40}Ca; for example, for a ^{40}Ca target, we have $Q(n, d) = -6.10$ MeV and $Q(p, d) = -13.41$ MeV leading to differences in momentum matching, transferred nucleon form factor, etc. For ^{16}O, the Q-value
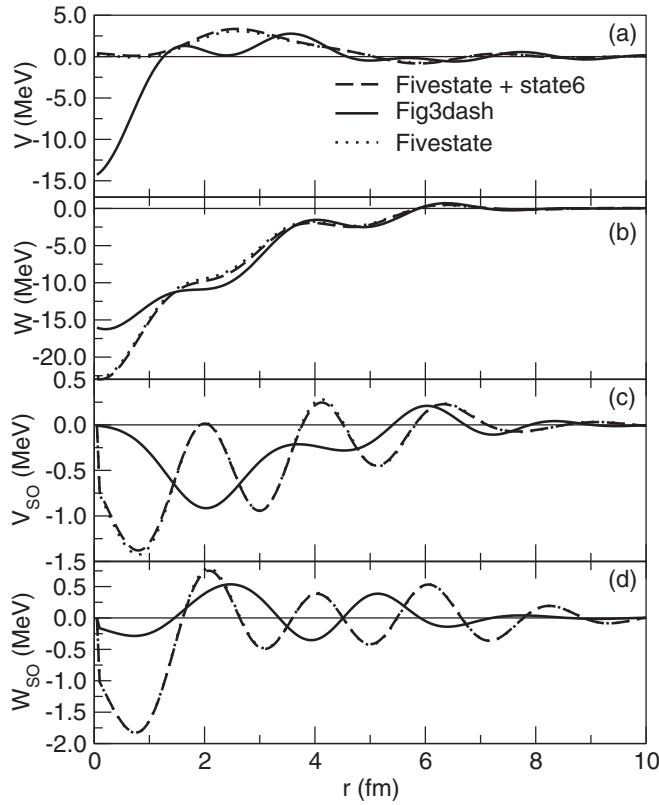
FIG. 6. For 30.3 MeV protons on ^{40}Ca, the dotted lines present the DPP due to coupling to the five lowest states. The dashed lines present the numerical sum of the DPP due to the five lowest states (the dotted lines) and the DPP for just state 6, 5/2+ at 8.5148 MeV. For comparison, the solid lines present the DPP with all six states coupled simultaneously, including state 6 together with the five lowest states, in a single CRC calculation. The Fig3dash DPP is almost indistinguishable from the All1 DPP. The panels present, from the top down, the real central, imaginary central, real spin-orbit, and imaginary spin-orbit components.

difference is between $Q(n, d) = -9.90$ MeV and $Q(p, d) = -13.44$ MeV, less than half the difference for ^{40}Ca. In what follows, we present CRC calculations of the DPP for the (n, d) cases listed in Table IV, the first two of which correspond to
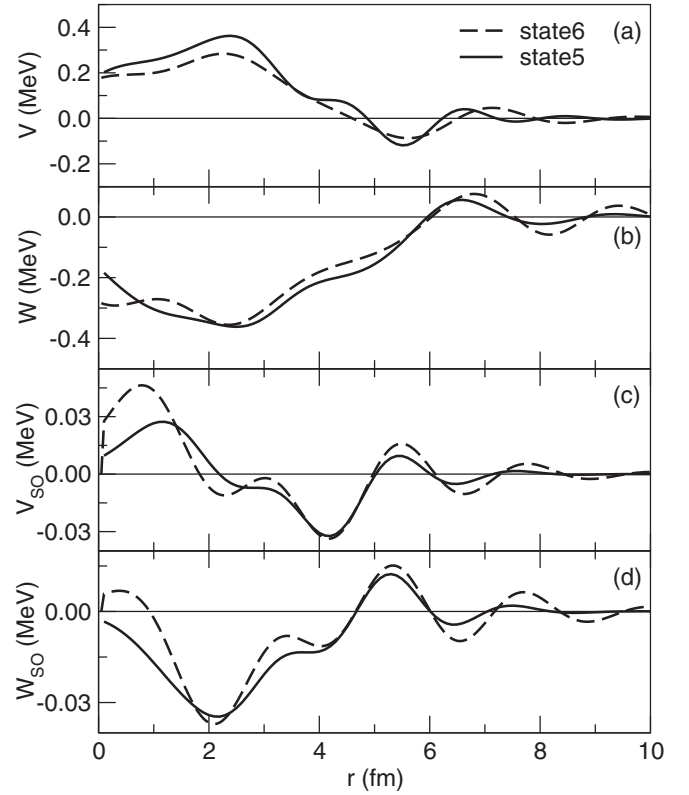
FIG. 7. For 30.3 MeV protons on ^{40}Ca, the solid lines present the DPP due to coupling to state 5, $\frac{5}{2}^+$ at 7.3148 MeV and the dashed lines present the DPP for state 6, $\frac{5}{2}^+$ at 8.5148 MeV. The spectroscopic factor for state 5 is the greater by a factor of 1.17. The panels present, from the top down, the real central, imaginary central, real spin-orbit, and imaginary spin-orbit components.

particular entries in Table I. We apply the same bare OMP parameters and the coupling is to the hole states in ^{39}K that correspond to those listed above for ^{39}Ca, with the appropriate measured excitation energies. For neutron scattering, the All1 calculations include couplings to the following states in ^{39}K : $\frac{3}{2}^+$ 0.0 MeV; $\frac{1}{2}^+$ 2.52 MeV; $\frac{7}{2}^-$ 2.82 MeV; $\frac{5}{2}^+$ 6.51 MeV. The $\frac{5}{2}^+$ state sums the strength of 7 actual $\frac{5}{2}^+$ states at

TABLE III. For protons scattering from ^{40}Ca at 30.3 MeV/nucleon, volume integrals ΔJ (in MeV fm^3) of the four components of the DPP induced by (p, d) coupling for the test cases referred to in Sec. IV C, plus the All1 case for comparison. The ΔR_{rms} column gives the change in rms radius of the real central component (in fm). The final three columns present, respectively, the change in the total reaction cross section induced by the coupling, the integrated cross section to the specific coupled reaction channels and the ratio R defined in the text. Note that negative ΔJ_R corresponds to repulsion. The quantities Δ(Reac CS) and State CS are given in mb. As in Table I, "4*(x MeV)" indicates a single lumped $\frac{5}{2}^+$ state at x MeV including the strength of all the $\frac{5}{2}^+$ states.

| Label	States coupled	ΔJ_R	ΔJ_{IM}	ΔJ_{RSO}	ΔJ_{IMSO}	ΔR_{rms}	Δ(Reac CS)	State CS	R
test1	1, 2, 3, 4*(3 MeV)	-17.82	64.71	4.018	-0.266	0.0835	148.03	17.56	2.29
test2	1, 2, 3, 4*(4 MeV)	-14.22	62.90	4.146	-0.757	0.0786	148.53	17.09	2.36
test3	1, 2, 3, 4*(5 MeV)	-12.10	60.02	4.146	-1.361	0.0619	148.43	16.46	2.47
test4	1, 2, 3, 4*(6 MeV)	-8.42	60.31	3.981	-1.811	0.0494	147.73	15.67	2.45
All1	1, 2, 3, 4*(6.5132 MeV)	-7.37	59.99	3.756	-1.736	0.0338	147.13	15.22	2.45
testX	1, 2, 3, 4*(10 MeV)	2.01	53.72	2.653	-2.585	0.0074	140.23	11.56	2.63
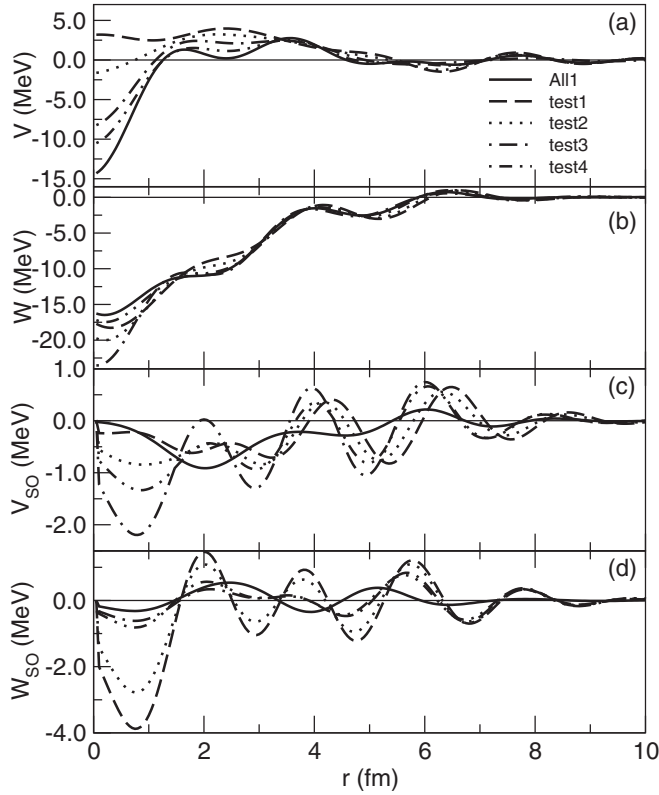
FIG. 8. For 30.3 MeV protons on ^{40}Ca, the solid lines present the DPP due to coupling to the set of states designated "All1." The dashed lines present the DPP for case "test1," the dotted lines for "test2," the dot-dashed lines for "test3," and the dash-dot-dot-dash lines for "test4," see text. The panels present, from the top down, the real central, imaginary central, real spin-orbit, and imaginary spin-orbit components.

FIG. 9. For 30.3 MeV protons on ^{40}Ca, the solid lines present the DPP due to coupling to the set of states designated "All1." The dashed lines present the DPP for case "testX," see text. The panels present, from the top down, the real central, imaginary central, real spin-orbit, and imaginary spin-orbit components.

the weighted mean excitation energy. The source is Ref. [5], as for the neutron hole states in ^{39}Ca in the (p, d) calculations.

The solid lines in Fig. 10 represent the DPP in the neutron potential generated by coupling to the first, $\frac{3}{2}^+$, state in ^{39}K. For comparison, the dashed lines show the DPP for the corresponding state for proton scattering. The qualitative shapes are very similar, indicating repulsion and absorption in each case. However, the conspicuous feature is the much smaller magnitude of each component of the neutron DPP compared with the corresponding component of the proton DPP. Both DPPs possess a region in the surface where they become emissive which may be diagnostic of an underlying l dependence. The qualitative similarity in shape between the
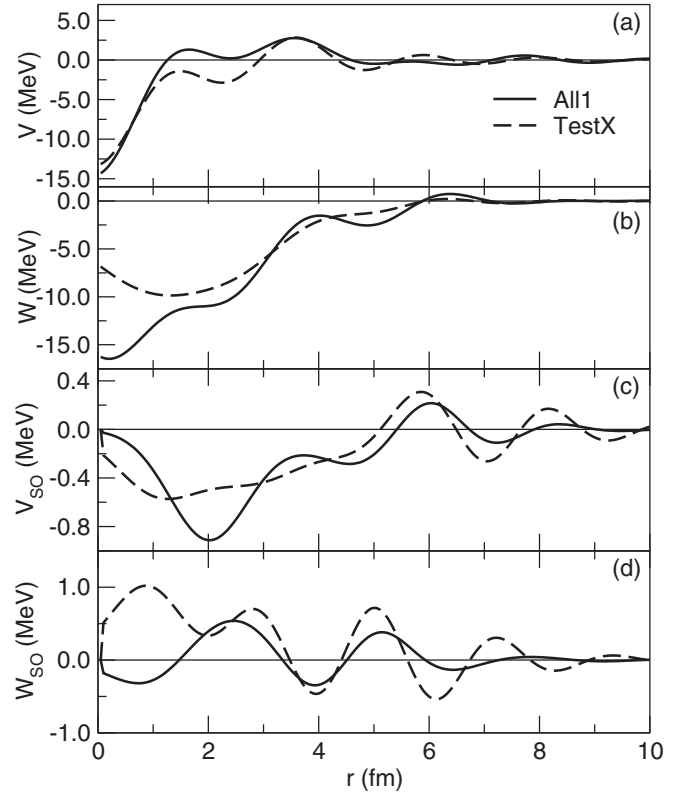
proton and neutron DPPs also applies to the small magnitude spin-orbit components.

This qualitative similarity between the proton and neutron DPPs does not apply to the All1 set of pickup states. The dashed lines in Fig. 11 represent the All1 DPP for neutron scattering. The components can be compared with those for the All1 case for protons, shown as solid lines. The imaginary central components have similar general shapes, but the depth is markedly less for neutrons, as it was for coupling to just the $\frac{3}{2}^+$ state. This corresponds to a much smaller value of ΔJ_{IM}, 44.22 MeV fm^3 for neutrons compared with 59.99 MeV fm^3 for protons coupled to the All1 set of states.

By contrast to the imaginary central components, the real central proton and neutron DPPs are qualitatively different: For neutrons it is repulsive for most of the radial range, whereas the real DPP for protons becomes sharply attractive

TABLE IV. For neutrons scattering from ^{40}Ca at 30.3 MeV/nucleon, properties of the DPP induced by (n, d) coupling. For symbols and units, refer to Table I.

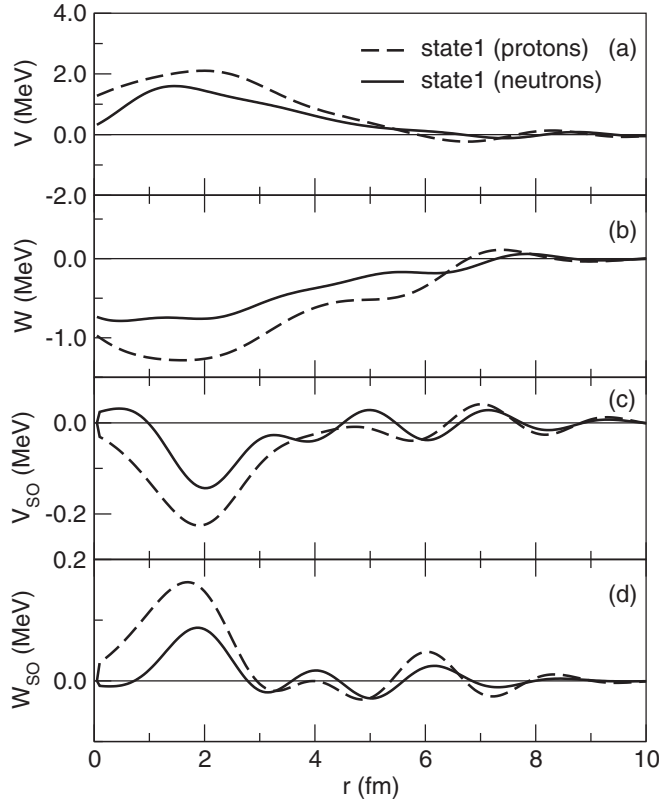| Label	States coupled	ΔJ_R	ΔJ_{IM}	ΔJ_{RSO}	ΔJ_{IMSO}	ΔR_{rms}	Δ(Reac CS)	State CS	R
GS	1	−10.59	8.75	0.444	−0.106	0.0138	41.1	8.12	4.69
All1	1, 2, 3, 4*(6.51 MeV)	−20.72	44.22	2.530	0.479	0.0464	159.6	27.78	3.61
All1-13p8	1, 2, 3, 4*(13.8 MeV)	−6.54	39.17	2.676	−0.908	0.0461	151.3	20.70	3.86

FIG. 10. For 30.3 MeV neutrons on ^{40}Ca, the solid lines represent the DPP due to coupling to the $\frac{3}{2}^+$ ground state of ^{39}K. The dashed lines represent the DPP for protons, coupling to the corresponding $\frac{3}{2}^+$ state in ^{39}Ca. The panels present, from the top down, the real central, imaginary central, real spin-orbit, and imaginary spin-orbit components.

FIG. 11. For 30.3 MeV neutrons on ^{40}Ca, the dashed lines present the DPP due to coupling to the set of states designated "All1." The solid lines represent the DPP for protons, case All1. The dotted lines represent the DPP for neutrons with modified excitation energy of the $\frac{5}{2}^+$ state, see text. The panels present, from the top down, the real central, imaginary central, real spin-orbit, and imaginary spin-orbit components.

for $r <$ about 1.3 fm. As a result, the coupling reduces the volume integral of the real neutron potential by 20.72 MeV fm^3 compared with a reduction of 7.37 MeV fm^3 for the proton potential. The change in shape is reflected in the values of ΔR_{rms} which for the All1 cases is 0.0338 fm for protons and 0.0464 fm for neutrons. It appears that single nucleon pickup induces differences between the volume integral, radial form and RMS radius for proton and neutron OMPs. For neutrons, the increase in reaction CS induced by the coupling is greater than for protons, whereas the change in imaginary volume integral is less for neutrons. Thus the ratio R is considerably greater for neutrons than for protons, a possible clue that we have not yet interpreted.

For protons, the attraction near the nuclear center was associated with the quite large negative Q value of the lumped $\frac{5}{2}^+$ state at 6.5132 MeV. To get some understanding of this, the CRC plus inversion procedure was repeated for neutrons with the All1 parameters with the important exception that the excitation energy of the lumped $\frac{5}{2}^+$ state was increased to 13.8 MeV. At this energy the Q value for this state is the same as for the corresponding (p, d) state. The result is given in the third row of Table IV and by the dotted lines in Fig. 11. With this change, the qualitative shape of the neutron potential resembles that for protons, with the deep attractive feature
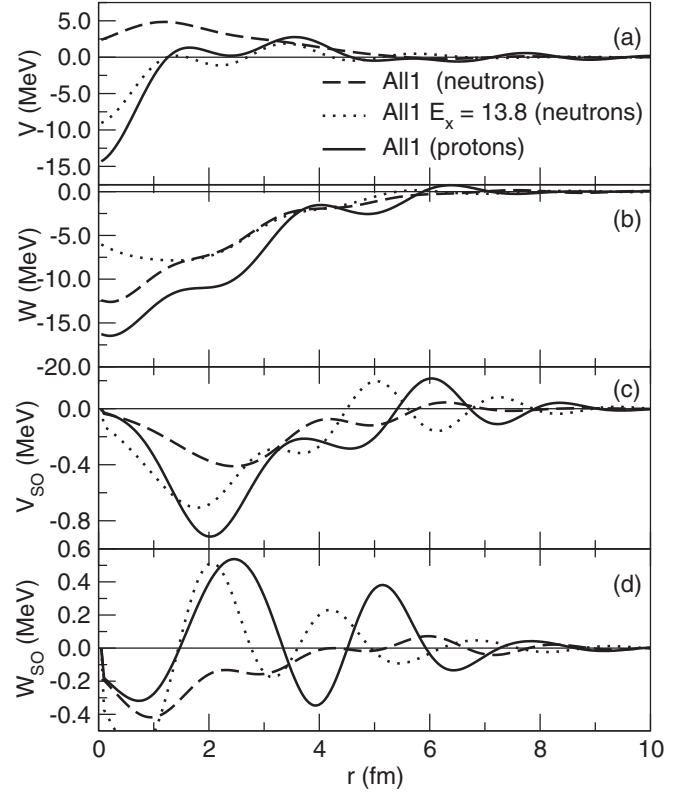
near the origin. By contrast, the imaginary part shows almost zero change for $r > 1$ fm. We have no full understanding of the strong short range attractive feature seen in the solid and dotted lines, but it is clearly linked to a large negative Q value.

VI. ENERGY DEPENDENCE: PROTON AND NEUTRON DPPS FROM 25 MEV TO 45 MEV

How atypical is the difference between proton and neutron DPPs found at 30.3 MeV or are such differences more general? Plausibly, the difference between the Q values for (p, d) and (n, d) will be less significant as the nucleon energy increases, reducing the charge symmetry breaking. We therefore carried out at 25, 35, 40, and 45 MeV the analysis applied at 30.3 MeV. In each case, the bare potential was that used at 30.3 MeV, justified by the independence of the DPPs to the details of the bare potential demonstrated in Ref. [16]. This allows all the changes presented here to be attributed to the energy. In each case, the coupling was to the All1 set of states. The resulting numerical properties for each energy are presented in Table V for both protons (P) and neutrons (N).

All quantities derived from S-matrix inversion vary monotonically with energy, with the exceptions of ΔJ_R (N) and ΔJ_{SOI} (N) for 40 MeV and 45 MeV, ΔJ_{SOR} (P) for 25 MeV,

TABLE V. For protons (P) and neutrons (N) scattering from ^{40}Ca at energies from 25 to 45 MeV, volume integrals ΔJ (in MeV fm^3) of the four components of the DPP induced by (p, d) or (n, d) coupling. Negative values of ΔJ_R indicate repulsion. The change in rms radius of the real potential, $\Delta R_{\rm rms}$, is given in fm. The quantities Δ(Reac CS) and State CS are given in mb.

Energy	25 MeV	30.3 MeV	35 MeV	40 MeV	45 MeV
ΔJ_R (P)	5.27	-7.37	-16.08	-20.85	-23.06
ΔJ_R (N)	-15.08	-20.72	-22.79	-22.62	-21.76
$\Delta R_{\rm rms}$ (P)	0.0024	0.0338	0.0516	0.0524	0.0458
$\Delta R_{\rm rms}$ (N)	0.0460	0.0464	0.0431	0.0367	0.0299
$\Delta J_{\rm IM}$ (P)	69.00	59.99	51.89	42.83	34.10
$\Delta J_{\rm IM}$ (N)	54.72	44.22	36.19	29.29	24.04
$\Delta J_{\rm SOR}$ (P)	3.22	3.76	3.12	2.34	1.74
$\Delta J_{\rm SOR}$ (N)	3.76	2.53	1.84	1.33	1.03
$\Delta J_{\rm SOI}$ (P)	-4.20	-1.74	-0.39	0.28	0.34
$\Delta J_{\rm SOI}$ (N)	-0.30	0.48	0.64	0.58	0.51
ΔReac CS (P)	147.7	147.1	142.9	130.9	115.1
ΔReac CS (N)	177.3	159.6	139.2	118.6	100.7
R (P)	2.14	2.45	2.75	3.06	3.38
R (N)	3.24	3.60	3.85	4.05	4.19
State CS (P)	7.62	15.2	19.8	22.5	23.2
State CS (N)	24.5	27.8	27.9	26.6	24.4

and some values of $\Delta R_{\rm rms}$. The differences between the values of ΔJ_R for protons and neutrons are largest at the lower energies, being about 20 MeV fm^3 at 25 MeV falling to a small value at 45 MeV. This would imply a different energy dependence for the proton and neutron OMPs over this energy range. The channel coupling results in a consistent increase in the effective real spin-orbit potential, but the effect is less for neutrons than for protons except at 25 MeV. The differences between $\Delta J_{\rm IM}$ are quite large at most energies, falling to 10 MeV fm^3 at 45 MeV.

The quantities ΔReac CS (the change in reaction cross section due to the pickup coupling) and "State CS" (the summed cross section to the coupled pickup states) are not dependent on the S-matrix inversion. ΔReac CS varies monotonically with energy, falling much more rapidly for neutrons. The quantity R is expected to change less rapidly than either $\Delta J_{\rm IM}$ or ΔReac CS as the energy or the coupling case changes. From Table V this is evidently the case. Although we have no quantitative argument for the sign of the energy dependence, the steady monotonic behavior is reassuring for the values of $\Delta J_{\rm IM}$ found by inversion.

In all cases the increase in reaction cross section generated by the pickup coupling is much greater than the pickup cross section itself. This suggests that the pickup channel serves as a doorway for other reactions. The surprisingly small pickup cross section for 25 MeV protons contrasts with the large corresponding $\Delta J_{\rm IM}$. This is probably related to the particular behavior of the proton DPP for 25 and 30.3 MeV and deserves further study, particularly regarding the nature of the deuteron OMP, which is fixed in all of these studies.

A. Radial dependence

The DPPs at each energy are presented in Fig. 12 for protons and Fig. 13 for neutrons. The anomalous attractive behavior of the proton DPP for small radii is obvious for both

25 MeV and 30.3 MeV; this does not occur for pickup to individual states with less negative Q values. In contrast, for neutrons there is repulsion at small radii for all energies, as
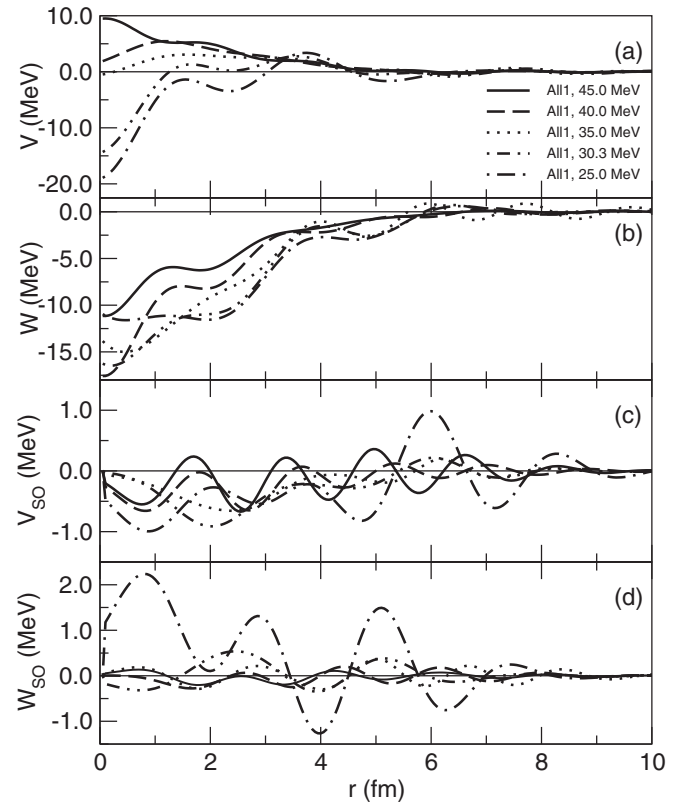

FIG. 12. For protons on ^{40}Ca for energies between 25 MeV and 45 MeV, the DPPs due to pickup coupling to the complete set of states in the All1 grouping. The panels present, from the top down, the real central, imaginary central, real spin-orbit, and imaginary spin-orbit components.

FIG. 13. For neutrons on ^{40}Ca for energies between 25 MeV and 45 MeV, the DPPs due to pickup coupling to the complete set of states in the All1 grouping. The panels present, from the top down, the real central, imaginary central, real spin-orbit, and imaginary spin-orbit components.
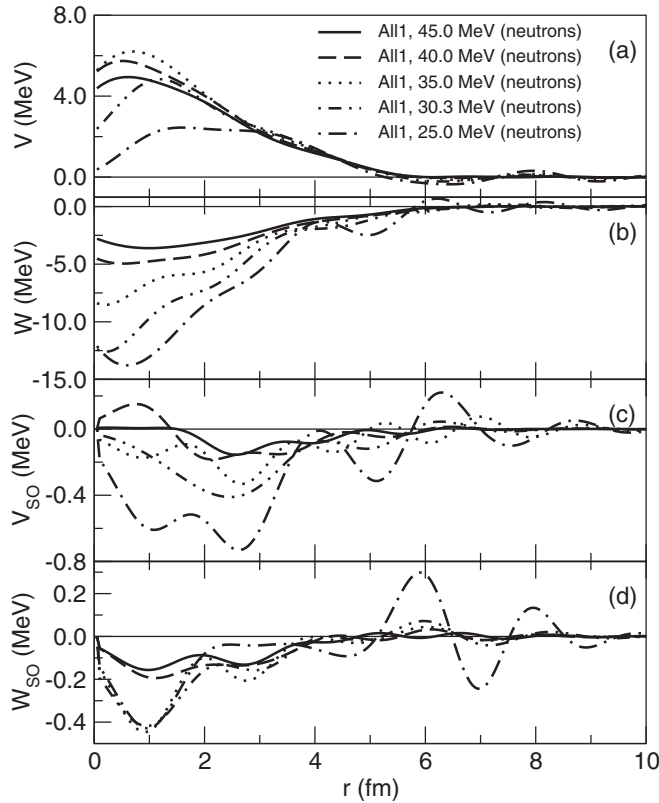
is evident in Fig. 13. This difference in low-r behavior at the lower energies for protons is reflected in the behavior of ΔJ_R which becomes closer for protons and neutrons at the higher energies. By contrast, the difference between $\Delta J_{\rm IM}$ for protons and neutrons appears to persist to 45 MeV.

At each of the three lower energies, there is evidence for an emissive region in the proton imaginary potential at about 6 fm. We comment on this in Sec. VIII. In this connection we note that fits to analyzing power data are essential for precisely establishing the central terms as well as the spin-orbit terms, and regret the near total lack of such data for neutron elastic scattering.

A quantitative measure of the radial dependence of the real part is the change in the rms radius, $\Delta R_{\rm rms}$. This is positive in every case, and generally varies steadily, except for protons at 25 MeV where ΔJ_R is also exceptional. At the higher energies $\Delta R_{\rm rms}$ is larger for protons than for neutrons. The systematically positive value for this quantity due to reaction channel coupling may be significant when folding models are invoked for the determination of nuclear radii using elastic scattering.

B. General comment

There is, of course, no escaping the constraints imposed by causality, but we currently have no suggestion as to how the

effects disclosed here can be straightforwardly incorporated with consistent dispersion relations.

VII. THE DIFFERENCES BETWEEN THE PROTON AND NEUTRON DPPS

Although for many purposes charge symmetry of nuclear interactions holds quite well, the effect of the Coulomb interaction can be magnified in direct reactions. The Q values for (γ, p) and (γ, n) for ^{40}Ca are -8.33 MeV and -15.64 MeV, respectively, hence the (n, d) and (p, d) Q values of -6.103 MeV and -13.41 MeV, respectively. This can affect pickup coupling effects in two ways: (1) through the difference in radial form factor for the transferred nucleon and (2) the difference in energy of the outgoing deuteron with the consequent changes in momentum transfer and absorption. Regarding (1), there is a low Coulomb barrier with proton transfer and this may contribute to the very different State CS values in Tables I and IV for the All1 case. Regarding (2), the deuteron energy can be significantly low for (p, d) reactions at 25 or 30 MeV. Both of these effects contribute to the charge symmetry breaking differences between the effective proton-nucleus and neutron-nucleus interactions that we have found.

To evaluate the significance of the coupling effects that we have found, we note that the standard phenomenological measure of the difference between proton and neutron global OMPs is that due to Perey [17]. The difference between the real central proton and neutron potential parameters (presumed Wood-Saxon) is given by $V_p - V_n = 0.4Z/A^{1/3}$, where V is positive by convention for an attractive potential. This term allows for the combined effect of the reduced kinetic energy of protons within the nucleus and the energy dependence of the nucleon OMP, due mostly to knock-on exchange. This recipe is appropriate over the energy range relevant to the present work. For a ^{16}O target, the proton potential would be about 1.27 MeV deeper than the neutron potential. For a ^{40}Ca target the proton OMP would be about 2.34 MeV deeper than the neutron OMP, corresponding to a difference of about 20.4 MeV fm^3 in the normalized volume integral. The differences, $J_R({\rm diff})$, between the volume integrals of the proton and neutron global potentials of Koning and Delaroche [18], KD, are substantial. For the energies of Table V, 25 MeV to 45 MeV, we find for $J_R({\rm diff})$: 40.94, 26.67, 26.37, 25.96, and 24.53 MeV fm^3, respectively. The differences for the imaginary KD potential, $J_I({\rm diff})$, at the same energies are: 4.64, 5.49, 6.12, 6.74, and 7.34 MeV fm^3. From Table V we find pickup induced values of $J_R({\rm diff})$ for the same energies of 20.35, 13.59, 6.71, 1.77, and -1.30 MeV fm^3. The pickup induced values of $J_I({\rm diff})$ at the same energies are: 14.28, 15.74, 15.70, 13.54, and 10.06 MeV fm^3.

From this perspective, the changes in terms of volume integrals of the real potential, ΔJ_R, resulting from the coupling to nucleon pickup channels, do not seem large (except at 25 MeV) although the difference between ΔJ_R values for protons and neutrons is significant at 30.3 MeV due to the changes in shape for small r. Values of ΔJ_R for both protons and neutrons become quite small at 40 MeV. However, ΔJ is far from the whole story and the effect of pickup coupling on

the radial shape is marked, particularly at the lower energies where the effect at small r is large, compare Figs. 12 and 13. There is a significant effect on the rms radius that is similar for protons and neutrons at 30.3 MeV. At that energy the effects on the imaginary central and spin-orbit potentials are substantially different for protons and neutrons. Above 30 MeV the coupling effect on the real spin-orbit potential is systematically less for neutrons.

A general result is that pickup coupling can be expected to affect the smooth energy dependence of the nucleon OMP in the energy range where coupling effects to pickup channels are strong. Pickup coupling appears systematically to increase the effective radius of the real potential, with two consequences: this cannot be corrected by renormalizing folding models, and could falsify the extraction of nuclear radii from fitting elastic-scattering data.

A. Other reaction channel couplings

Although we do not investigate the effect of two-nucleon transfers in the present study, we note large variations in Q values: For protons, the Q value for (p, t) is -20.45 MeV and for $(p, {}^3\text{He})$ is -13.69 MeV, whereas for neutrons the Q value for (n, t) is -12.92 MeV and for $(n, {}^3\text{He})$ is -6.99 MeV. Although these transfer reactions are not likely to have large cross sections, the effect on elastic scattering might not be small. We note the quite small values of State CS in Table I for single nucleon coupling.

VIII. REMARKS ON UNDULARITY, EMISSIVENESS, AND l DEPENDENCE

In general, the inverted potentials exhibit undularity which, in some cases, leads to emissive regions in the imaginary component of the potential. This does not give rise to any breaking of the unitarity limit $|S_{lj}|^2 \leqslant 1$. This is guaranteed by the reaction channel calculation for which the limit holds. Such emissive regions appear in proton elastic-scattering phenomenology in which potentials have been fitted to angular distributions and analyzing powers that are precise and of wide angular range.

For certain nuclei, particularly closed shell nuclei such as ${}^{16}\text{O}$ and ${}^{40}\text{Ca}$, for which data of exceptional precision and angular range exist, no smooth, Woods-Saxon-like, potential can be found that precisely fits such data. Two alternative ways of fitting the data do, however exist: l-dependent potentials [19] and undulatory potentials as obtained by model independent fits (splines, sums of Gaussians, Bessel functions, etc.), see, for example, Ref. [20]. A wide range of data can be fitted with either approach. They can be viewed as alternatives since the S_{lj} from any l-dependent potential can be inverted, in general leading to an undulatory l-independent potential. The message to be taken from this is that the undulations that we find are indicative of an underlying DPP that is, in fact, l dependent. That is fine, since the formal DPPs have this property [7–9].

There are few systematic model independent fits to nucleon-scattering data, in part because of a lack of data of appropriate quality. The existing study [20] that is relevant to the present case does find undulations, but is defective in a way that is instructive here. The so-called theoretically unprejudiced fits of that study did, in fact, have a prejudice: there was a constraint that the imaginary part would not become negative for any r. We now know that this is an inappropriate constraint. Our statement above that emissive regions appear in precise phenomenology is based on the fact that l-dependence is required to fit such data, and the l-independent S-matrix equivalent to such a potential will exhibit undularity and regions of emissivity, as is also the case with some DPPs arising from CRC calculations.

IX. SUMMARY, CONCLUSIONS, AND WHAT NEXT?

Coupling to deuteron channels substantially modifies the interaction between nucleons and nuclei: The coupling generates a substantial DPP. The properties of this DPP are not compatible with the smooth Woods-Saxon-like form of standard phenomenology or folding models based on a local density approximation. For all terms of the DPP, real and imaginary, central and spin-orbit, the results for neutrons and protons are significantly different.

A. Central potential

For proton scattering, the real central part of the DPP has a radial form incompatible with a uniform renormalization of a folding model potential derived from a local density model. For 30.3 MeV protons, pickup of the deeper lying neutrons generated a distinctive change in the radial form of the real central DPP for small radii, leading to reduced repulsion as measured by ΔJ_R. This distinctive effect of the deeper lying neutron hole states is also apparent in Table II where the sign of the difference between the "summed" and "together" values of ΔJ_R in the first two listed cases is the opposite of that in the last three listed cases which involve pickup of the more deeply lying neutrons.

For proton scattering, at the higher of the energies considered here, the volume integral of the real central DPP indicates a net repulsive effect that varies with energy in a regular way. It is less regular at the lower energies, about 25–30 MeV. At 25 MeV the volume integral indicates a net attractive effect due to a strongly attractive region near the nuclear center. The imaginary potential, on the other hand, decreases with energy in a completely regular way with ΔJ_{IM} halving between 25 and 45 MeV incident energy. Adding reaction channels always increased the magnitude of ΔJ_{IM}; this was not the case for changes in ΔJ_R.

For neutrons, the real central DPP is repulsive at all energies studied, apart from some shallow attraction in the surface, around 6.5 fm. As was the case for protons, the radial form would not correspond to a uniform renormalisation of a folding model potential. For energies of 25–35 MeV the neutron DPP, as quantified by ΔJ_R, is considerably more repulsive than for protons, to a large degree at 25 MeV. The difference is small at 40–45 MeV.

B. Spin-orbit potential

For both protons and neutrons the real part of the spin-orbit interaction is consistently enhanced by the coupling. The spin-orbit DPPs are quite undulatory, but the volume integrals appear to represent the overall effect well, and vary consistently with energy. The bare potential of the present calculations had no imaginary spin-orbit component and for both protons and neutrons the coupling generates an imaginary spin-orbit term that is overall negative at the lowest energy (25 MeV), becoming positive as the energy increases.

C. General properties

All components of the DPP have some degree of undularity, with some local regions where the imaginary terms become emissive. This does not lead to any breaking of the unitarity limit.

D. Energy dependence

The properties of the DPPs given in Table V vary regularly with increasing energy. The actual changes suggest that the properties of OMPs, fitted to precise data of wide angular range, would show some discontinuity around 25–30 MeV for which the outgoing deuterons have low energy. Indeed, a single calculation for neutrons at 22.8 MeV followed the trend of Fig. 13, with the real DPP becoming attractive near $r = 0$. For all energies, the properties of the proton DPP near $r = 0$ differed from the neutron DPP, but they agreed insofar as both showed increasing attraction (or decreasing repulsion) in this radial region with decreasing energy.

E. Q-value dependence

The form of the DPP was very sensitive to the Q value for the transfer to the $\frac{5}{2}^+$ state, as can be seen from the "Test" series of cases reported in Table III and Fig. 8. The difference between the proton and neutron DPPs was illuminated by the DPPs shown in Fig. 11 where it was demonstrated that when the Q value for (n, d) coupling to the $\frac{5}{2}^+$ state was adjusted to equal that for the (p, d) case, the real DPP near $r = 0$ was very similar to that for protons at the same energy.

F. Links to experiment

At present, it is difficult establish a direct link between the effects of pickup coupling and experiment. Fitting experimental elastic-scattering data by searching on the full set of bare potential parameters is barely practicable for CRC calculations with the full set of reaction channels.

There is only an indirect relationship between our results and existing experiments. The precise data of Ref. [21,22] for protons on ^{40}Ca at 30.3 MeV cannot be fitted with smooth, Woods-Saxon-like potentials, but can be fitted with, alternatively, an l-dependent potential [19], an undulatory potential [20], or even what we now see as deficient deuteron-coupling CRC calculations [23,24]. What is certain is that an l-independent potential that exactly fits the data must be, to some degree, undulatory.

Unfortunately, a verification of the proton-neutron differences is currently not possible due to the lack of appropriate neutron data, analyzing power data in particular. The interesting details suggested here cannot be tested in the absence of quality analyzing power data for neutrons. We are aware that accurate analyzing power measurements are difficult for neutrons, but the absence of such data is a barrier to a full understanding of nucleon-nucleus interactions.

It is now more than half a century since the precision measurements of Ref. [21]; it is to be hoped that the challenge of providing more and better such data will be taken up since there is much concerning the interaction of nucleons and nuclei that is still not understood, as the present work indicates.

G. What next?

Many processes are still omitted in the calculations presented here. For example, it is known that the coupling to collective states is important [25]. Inclusion of these is probably the next step, but fitting data by searching on the parameters of a bare potential when both reaction channel coupling and collective coupling are included is computationally challenging. Another avenue for exploration is to compare the DPPs found by CRC plus inversion with the model independent additive correction to realistic folding model potentials [26], as determined by fitting precise data. There is always the possibility of double counting between the particle-hole contributions to a folding model and the pickup coupling contribution. However, if any folding model does not lead to an undulatory potential, the DPPs we have found suggest that it is incomplete.

Our results are a direct challenge to the customary assumption that the nucleon-nucleus potential is both l-independent and smooth (Woods-Saxon like, with no undularity) and calculable with a local density model.

[1] N. Keeley and R. S. Mackintosh, Phys. Rev. C **97**, 014605 (2018).

[2] R. S. Mackintosh and N. Keeley, Phys. Rev. C **76**, 024601 (2007).

[3] R. S. Mackintosh and N. Keeley, Phys. Rev. C **81**, 034612 (2010).

[4] N. Keeley and R. S. Mackintosh, Phys. Rev. C **83**, 044608 (2011).

[5] R. S. Mackintosh and N. Keeley, Phys. Rev. C **85**, 064603 (2012).

[6] R. S. Mackintosh and N. Keeley, Phys. Rev. C **97**, 069901(E) (2018).

[7] H. Feshbach, Ann. Phys. **5**, 357 (1958); **19**, 287 (1962).

[8] G. H. Rawitscher, Nucl. Phys. A **475**, 519 (1987).

[9] G. R. Satchler, *Direct Nuclear Reactions* (Clarendon Press, Oxford, 1983).

[10] N. Keeley and R. S. Mackintosh, Phys. Rev. C **90**, 044602 (2014).

[11] F. G. Perey and B. Buck, Nucl. Phys. **32**, 353 (1962).

[12] F. G. Perey, in *Direct Interactions and Nuclear Reaction Mechanisms*, edited by E. Clemental and C. Villi (Gordon & Breach, New York, 1963), p. 125.

[13] R. S. Mackintosh and S. G. Cooper, J. Phys. G: Nucl. Part. Phys. **23**, 565 (1997).

[14] I. J. Thompson, Comput. Phys. Rep. **7**, 167 (1988).

[15] R. S. Mackintosh and N. Keeley, arXiv:1610.07378.

[16] R. S. Mackintosh and N. Keeley, Phys. Rev. C **98**, 024624 (2018).

[17] F. G. Perey, Phys. Rev. **131**, 745 (1963).

[18] A. J. Koning and J. P. Delaroche, Nucl. Phys. A **713**, 231 (2003).

[19] R. S. Mackintosh, arXiv:1302.1097v5.

[20] A. M. Kobos and R. S. Mackintosh, Ann. Phys. (NY) **123**, 296 (1979).

[21] B. W. Ridley and J. F. Turner, Nucl. Phys. **58**, 497 (1964).

[22] V. Hnizdo, O. Karban, J. Lowe, G. W. Greenlees, and W. Makofske, Phys. Rev. C **3**, 1560 (1971).

[23] R. S. Mackintosh, Phys. Lett. B **44**, 437 (1973).

[24] R. S. Mackintosh and A. M. Kobos, Phys. Lett. B **62**, 127 (1976).

[25] R. S. Mackintosh and N. Keeley, Phys. Rev. C **90**, 044601 (2014).

[26] R. S. Mackintosh, Eur. Phys. J. A **53**, 66 (2017).